Check for updates

JGR Oceans

RESEARCH ARTICLE
10.1029/2024JC021126

Flow Evolution and Vertical Accelerations in Wave-Swash Interactions

Claudio Meza-Valle[1] and **Nimish Pujara**[1]

[1]Department of Civil and Environmental Engineering, University of Wisconsin-Madison, Madison, WI, USA

Key Points:

- Wave-swash interactions can be characterized by the ratio of consecutive wave heights and the dimensionless time separation between them
- Large upward-directed vertical accelerations that often exceed gravity are observed for certain wave-swash interactions
- During large upward-directed vertical accelerations, the flow velocity is upward- and onshore-directed

Correspondence to:
C. Meza-Valle,
meza4@wisc.edu

Citation:
Meza-Valle, C., & Pujara, N. (2024). Flow evolution and vertical accelerations in wave-swash interactions. *Journal of Geophysical Research: Oceans*, *129*, e2024JC021126. https://doi.org/10.1029/2024JC021126

Received 18 MAR 2024
Accepted 18 SEP 2024

Author Contributions:
Conceptualization: Nimish Pujara
Data curation: Claudio Meza-Valle
Formal analysis: Claudio Meza-Valle, Nimish Pujara
Funding acquisition: Nimish Pujara
Investigation: Claudio Meza-Valle
Methodology: Claudio Meza-Valle, Nimish Pujara
Project administration: Nimish Pujara
Resources: Nimish Pujara
Software: Claudio Meza-Valle, Nimish Pujara
Supervision: Nimish Pujara
Validation: Claudio Meza-Valle
Visualization: Claudio Meza-Valle
Writing – original draft: Claudio Meza-Valle
Writing – review & editing: Nimish Pujara

© 2024. The Author(s).
This is an open access article under the terms of the Creative Commons Attribution-NonCommercial-NoDerivs License, which permits use and distribution in any medium, provided the original work is properly cited, the use is non-commercial and no modifications or adaptations are made.

Abstract We report on a laboratory study of wave-swash interactions, which occur in the very nearshore environment of a beach when the shallow swash flow of a breaking wave interacts with a subsequent wave. Wave-swash interactions have been observed in the field, hypothesized to be important for nearshore transport processes, and categorized into different qualitative types, but quantitative descriptions of their dynamics have remained elusive. Using consecutive solitary waves with different wave heights and separations, we generate a wide variety of wave-swash interactions with large flow velocities and vertical accelerations. We find that wave-swash interactions can be quantitatively characterized in terms of two dimensionless parameters. The first of them corresponds to the wave height ratio for consecutive waves, and the second is a dimensionless measure of the time separation between consecutive wave crests. Using measurements of bed pressure and free-surface displacement, we estimate the total vertical accelerations and focus on the peak upward-directed acceleration. We find that wave-swash interactions can generate vertical accelerations that can easily exceed gravity, despite occurring in very shallow water depths. The large vertical accelerations are upward-directed and are quickly followed by onshore-directed horizontal velocities. Together, our findings suggest that wave-swash interactions are capable of inducing large material suspension events of sediment or solutes in sediment pores, and transporting them onshore. While the data are from a single location making it difficult to generalize the findings across the swash zone, the results clearly demonstrate the importance of large vertical accelerations in wave-swash interactions.

Plain Language Summary Waves arriving at a beach create fast shallow flows that are responsible for moving large amounts of sediment. Here, we consider how the flow due to one wave interacts with the next wave to arrive in idealized wave tank experiments. We find that in such interactions, flows moving in opposite directions can collide and create large, but short-lived peaks in upward-directed flow and acceleration. These peaks in flow and acceleration are likely to drive movement of material such as sediment and dissolved constituents in ways that are currently not taken into account.

1. Introduction

Water waves continuously shape sandy coastlines through sediment transport across a wide range of timescales, from sediment suspension events caused by individual waves to beach morphology changes that occur over seasons or years (e.g., Martínez et al., 2018; Toimil et al., 2020). Hydrodynamically, waves transformation near the coast is classified into several sub-regions such as the surf zone and swash zone (Dean & Dalrymple, 2004; Holthuijsen, 2007; Jackson & Short, 2020). In the swash zone, flow begins with the shoreward acceleration of the shoreline with the arrival and collapse of each wave, and is characterized by the movement of water up and down the beach, delimited by a cycle of upwash and backwash, otherwise referred to as a swash event (Brocchini & Baldock, 2008). In particular, wave-swash interactions are events where incoming waves collide with the upwash or backwash flows of the previous swash event. Wave-swash interactions have been qualitatively described in the field (e.g., Erikson et al., 2005; Hughes & Moseley 2007) and hypothesized to be an important mechanism for sediment transport (e.g., Alsina et al., 2009; Elfrink & Baldock, 2002; Puleo & Butt, 2006; Puleo & Torres-Freyermuth, 2016; Puleo et al., 2000) for some time.

The qualitative descriptions and types of wave-swash interactions include: (a) Wave-upwash interactions, where the upwash flow of a wave catches the upwash flow of the previous wave; (b) Weak wave-backwash interactions, where the upwash flow of a wave catches with the backwash flow of the previous wave, with the result that the flow is again pushed shoreward; and (c) Strong wave-backwash interactions, which are physically similar to weak wave-backwash interactions, but with result that the interaction induces a stop or receding of the incoming flow, often accompanied by a stationary hydraulic jump. In many field scenarios, the development of "free swash

21699291, 2024, 10, Downloaded from https://agupubs.onlinelibrary.wiley.com/doi/10.1029/2024JC021126 by Nimish Pujara - University Of Wisconsin , Wiley Online Library on [14/10/2024]. See the Terms and Conditions (https://onlinelibrary.wiley.com/terms-and-conditions) on Wiley Online Library for rules of use; OA articles are governed by the applicable Creative Commons License

events" (no interactions) tend to occur on the upper beach, whereas wave-swash interactions are common in the lower beach. For an incident wave train with constant wave heights, the time between wave crests relative to the timescale of the swash event has been used to understand these interactions (Baldock & Holmes, 1999; Lo et al., 2013; Pujara et al., 2015b), but this has been insufficient to understand the broad class of wave-swash interactions observed in the field for irregular waves (Chardón-Maldonado et al., 2016). W. Chen et al. (2023), in their recent extensive review of sediment transport models, concluded that even though there is an acceptance that wave-swash interactions play a critical role in the sediment transport in the swash zone, there are no parameters to determine the interaction type or the resulting sediment transport.

Interest in wave-swash interactions also stems from the observations that suggest wave-swash interactions could develop vertical (non-hydrostatic) pressure gradients and associated accelerations that trigger sediment liquefaction in the surf and swash zones (Elfrink & Baldock, 2002; Florence et al., 2022; Puleo & Butt, 2006; Puleo & Torres-Freyermuth, 2016; Stark et al., 2022), which would then lead to large sediment transport events. However, no framework exists for predicting when and if such liquefaction occurs. Indeed, some field observations suggest that wave-swash interactions that seem to follow very similar flow patterns produce sediment transport in opposite directions (Masselink et al., 2009). Similarly, output of numerical models for predicting beach morphology changes (e.g., Smit et al., 2010), when compared with controlled laboratory experiments, show that while the hydrodynamic variables are well predicted, the suspended sediment concentrations are not, especially during wave-swash interactions (Mancini et al., 2021; Ruffini et al., 2020). Thus, even when sediment transport mechanisms such as bedload and suspended sediment transport are implemented, they appear to lack important aspects of the flow and acceleration.

In this work, we use controlled experiments in a wave flume to find quantitative descriptions of wave-swash interactions. Our method considers the generation solitary waves since they travel without change of form (ignoring small viscous losses (Liu et al., 2007)) and generate large swash events whose properties can be understood in terms of a small set of input parameters (Pujara et al., 2015a). By generating two consecutive solitary wave events, we can set the strength of the first swash event through the wave height of the first wave and set the wave height and arrival time of the second wave through its height and separation from the first wave, thereby providing full control of the wave-swash interaction. This approach complements previous experiments using regular waves, bi-chromatic waves, solitary waves, and dam-break bores to understand and flow and transport in the swash zone (Alsina et al., 2009, 2012, 2016, 2018; Barale et al., 2024; Barranco & Liu, 2021; B.-T. Chen et al., 2016; Kikkert et al., 2012; Lo et al., 2013; O'Donoghue et al., 2010, 2016; Park, 2009; Pintado-Patiño et al., 2021; Pujara et al., 2015b; Sou & Yeh, 2011; Wu et al., 2021). By mimicking the interactions observed in the field, we analyze the main kinematic properties of wave-swash interactions, focusing in particular on the vertical accelerations and their correlation with the flow evolution. We find that there are large upward-directed vertical accelerations for certain interactions that cluster together when mapped onto two dimensionless parameters that can also predict different wave-swash interaction types.

The remainder of this manuscript is structured as follows. Section 2 presents the description of the experimental setup, including wave generation and instrumentation, Section 3 contains the results and analysis for swash events driven by single solitary waves and wave-swash interactions driven by consecutive solitary waves, and the concluding remarks are given in Section 5.

2. Laboratory Experiments

2.1. Wave Flume Setup

Experiments were conducted in a wave flume at the Water Science and Engineering Laboratory (WSEL) of the University of Wisconsin-Madison (Figure 1). The WSEL flume (39 m length, 0.9 m width, and 1.1 m height) is equipped with a piston-type wavemaker controlled by AwaSys (Aalborg University, Denmark) at one end and an impermeable smooth beach with a slope of 1:10 at the other end. The water depth was kept constant throughout the experiments at $h = 0.3$ m. Swash events and wave-swash events were generated using solitary waves. We place the origin of the lab coordinate system at a distance of 23.5 m from the wave paddle at the still water line (SWL) on the beach, with x pointing onshore and z pointing upwards against the acceleration of gravity.

Measurements of both the free-surface displacement, η, and the flow velocity (u,v,w) were taken at two control points, one in a constant depth at $x = -8.83$ m (CP_1) and one in the wave-swash interaction zone at $x = -0.3$ m

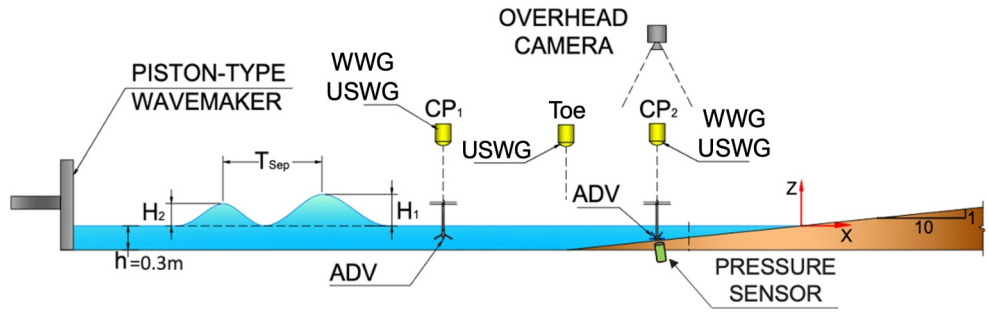

Figure 1. Experimental setup sketch.

(CP_2), and additional measurements of the free-surface displacement were taken at the toe of the beach ($x = -3$ m). At CP_2, a custom pressure transducer (Omega PX409 series with accuracy of 0.08% FS and a response time of <1 ms) was installed with the sensor face flush with the beach surface to measure the bed pressure. The free-surface displacement was measured at CP_1 and CP_2 using ultrasonic acoustic wave gauges (USWG; Senix ToughSonic-3 with 1 mm accuracy) and wire wave gauges (WWG, HR Wallingford with 0.1 mm accuracy) whereas only an ultrasonic wave gauge was used at the beach toe. The WWG calibration is prone to drift and thus the WWGs were calibrated at the start of every day when experiments were run whereas the USWG calibration is much more stable and only required calibration once before the start of the experiments. While both sensor types can be expected to give reliable data in the offshore regions where the wave slopes are mild, the WWG has better accuracy and is able to reliably measure the free-surface displacement with steep wave slopes due to wave breaking at CP_2 that the USWG is unable to measure. However, the WWG has a non-linear calibration response for shallow depths ($(\eta + h_{CP_2}) \leq 2$ cm), and we remove data below this threshold water depth, where $h_{CP_2} \approx 3$ cm is the local water depth at CP_2. In the analysis below, we use the WWG data at CP_1 and CP_2 and the USWG data at the beach toe. Data collection from all in situ instruments was synchronized and recorded at a sampling frequency of 50 Hz using a data acquisition system (NI 9205 and cDAQ-9185).

Acoustic Doppler velocimeters (ADVs, Nortek Vectrino Plus with accuracy of 1% FS) were used to measure all three components of the flow velocity at CP_1 (down-looking probe) and CP_2 (side-looking probe) with sampling volumes positioned at 15 and 0.75 cm above the bed, respectively, at a sampling frequency of 50 Hz. For data quality and control, we only report data with a signal-to-noise ratio (SNR) greater than 12 and a correlation value (CORR) greater than 70. Finally, two overhead cameras (JAI GO-5100-USB, 2,464 × 2,056 px, 8 bit resolution) fitted with 8 mm lenses (Thor labs) were mounted above the flume to record images over a combined field of view (FOV) of $x = [-70, 10]$ cm at 33.3 Hz. Data collection from the ADVs and cameras were synchronized with the remaining sensors by using the start of the wave paddle motion to trigger data collection.

2.2. Wave Conditions

Single and consecutive solitary waves were used in the experiments to generate single swash events and wave-swash interaction events, respectively. The wave paddle trajectory for single solitary waves uses Goring's theory (Goring, 1979), but the paddle trajectory for consecutive solitary waves was calculated by AwaSys using Boussinesq wavemaker theory backward in time to create the desired free-surface elevation timeseries at a specified location. As an input to this system, we constructed a timeseries of consecutive solitary waves to be realized at CP_1 using the Boussinesq solution for solitary waves (Boussinesq, 1872) with the wave peaks separated by a nominal separation time, T_{sep}. Measurements of the free-surface displacement and flow velocity at CP_1 compared well with the Boussinesq solution, which showed that the wave generation was robust for producing single and consecutive solitary waves. Additionally, we assessed the experimental repeatability by repeating specific cases covering different wave-swash interaction types five times, which showed the data were very repeatable, as has been previously observed in these type of experiments (Pujara et al., 2015b).

For consecutive solitary waves, we were able to independently control the height of each wave and the separation between them to produce different wave-swash interactions types as observed, categorized, and described by Hughes and Moseley (2007) and others in the field. These are wave-uprush interaction (WUI), where the second wave crest has delayed breaking and collapse as it propagates further onshore over a layer of uprush flow

21699291, 2024, 10, Downloaded from https://agupubs.onlinelibrary.wiley.com/doi/10.1029/2024JC021126 by Nimish Pujara - University Of Wisconsin , Wiley Online Library on [14/10/2024]. See the Terms and Conditions (https://onlinelibrary.wiley.com/terms-and-conditions) on Wiley Online Library for rules of use; OA articles are governed by the applicable Creative Commons License

generated by the swash of the first wave crest; weak wave-backwash interaction (WWBI), where the second wave crest encounters the backwash flow of the swash of the first wave, inducing accelerated breaking and collapse; and strong wave-backwash interaction (SWBI), where a stationary bore is generated by sudden breaking of the second wave crest as it encounters the strong backwash flow of the swash of the first wave.

The wave conditions covered single solitary waves with wave heights $H = [0.1, 0.2, 0.3, 0.4]h$ and consecutive solitary waves with $H_{1,2} = [0.1, 0.2, 0.3, 0.4]h$ and $T_{sep} = [0.75, 1.0, 1.25, 1.50, 1.75, 2.0]T_{H_1}$ where H_1 is the wave height for the first wave, H_2 is the wave height for the second wave, and T_{H_1} is the (effective) wave period of the first wave. There are four cases of single solitary waves and 60 cases of consecutive solitary waves. Table 1 presents a complete list of the 60 cases of consecutive solitary wave experiments. Of these 60 cases, 48 cases are analyzed below. In the remaining cases (marked with * in Table 1), the minimum water depth during the wave-swash interaction was below the threshold for reliable measurements with the wire wave gauge. For each case, we list the observed wave-swash interaction type, the wave height ratio (H_2/H_1) and the dimensionless separation time (T_{sep}/T_{swash}). The wave height and separation time measurements were made by first using a Gaussian kernel low pass filter (Mordant et al., 2004; Pujara et al., 2021) to the surface elevation measurements to reduce noise and simplify finding the peak of the free-surface displacement signal. The wave height ratio and dimensionless separation time are reported from measurements at CP_1, which is considered to be the "far field" or "input" condition, and CP_2, which is considered to be the "local" condition within the wave-swash interaction. Though the wave height ratio and dimensionless time separation could evolve in the constant depth region due to the differences in the phase speed and interactions between consecutive solitary waves, we have checked that this evolution is small and that these ratios have similar values at CP_1 and the beach toe.

2.3. Vertical Accelerations

We inferred the (total) vertical accelerations at CP_2 using data of the bed pressure and surface elevation. To do so, we start with the vertical component of the Navier-Stokes equation

$$\frac{Dw}{Dt} = -\frac{1}{\rho}\frac{\partial p}{\partial z} - g + \nu\nabla^2 w, \tag{1}$$

where w is the velocity in the z (vertical) direction, g is the gravitational acceleration, ρ is the fluid density, and ν is the kinematic viscosity. The viscous term $\left(\nu\nabla^2 w\right)$ was neglected under the assumptions that its influence is small over the bulk of the water column except in thin boundary layers adjacent to the bed and the free surface. In turbulent flow, the vertical velocity and the pressure above would be replaced by their corresponding Reynolds-averaged values and there would be an additional term related to the divergence of the Reynolds stress. The magnitude of the Reynolds stress term is likely to be much larger than the viscous term, but we neglect it under the assumption that the dominant momentum balance in the vertical direction is governed by the wave-driven mean (Reynolds-average) flow. This assumption needs to be verified more carefully in future work.

Next, assuming that the pressure varied linearly with depth in the shallow swash flow at CP_2, the vertical pressure gradient was approximated in terms of the difference between the surface pressure and bed pressure. Together, these assumptions reduce Equation 1 to

$$\frac{Dw}{Dt} \approx -\frac{1}{\rho}\frac{\left(p_{surface} - p_{bed}\right)}{(\eta + h_{CP_2})} - g = \frac{p_{bed}}{\rho(\eta + h_{CP_2})} - g, \tag{2}$$

where $p_{surface} = 0$ in gauge pressure, p_{bed} is the bed pressure, and $(\eta + h_{CP_2})$ is the total local water depth at CP_2. Thus, we can infer the total vertical accelerations from simultaneous measurements of the total water depth and the bed pressure. Note, only non-hydrostatic pressure distributions lead to vertical accelerations since the vertical acceleration vanishes $(Dw/Dt = 0)$ if the pressure distribution is hydrostatic $\left(p_{bed} = \rho g(\eta + h_{CP_2})\right)$. This estimate of the vertical acceleration can also be thought of as the kinematic non-hydrostatic vertical pressure gradient.

21699291, 2024, 10, Downloaded from https://agupubs.onlinelibrary.wiley.com/doi/10.1029/2024JC021126 by Nimish Pujara - University Of Wisconsin , Wiley Online Library on [14/10/2024]. See the Terms and Conditions (https://onlinelibrary.wiley.com/terms-and-conditions) on Wiley Online Library for rules of use; OA articles are governed by the applicable Creative Commons License

Table 1
Experimental Cases, Wave Parameters, Characteristic Ratios at Different Locations, and Type of Interaction Observed

Cases	$(H_2/H_1)_{CP_1}$	$(T_{sep}/T_{swash})_{CP_1}$	$(H_2/H_1)_{CP_2}$	$(T_{sep}/T_{swash})_{CP_2}$	Type
$H_1 = 0.1h; H_2 = 0.4h; T_{sep} = 0.75T_{H_1}$	3.57	0.5	3.25	0.3	WUI
$H_1 = 0.2h; H_2 = 0.3h; T_{sep} = 0.75T_{H_1}$	1.45	0.4	1.75	0.3	WUI
$H_1 = 0.2h; H_2 = 0.4h; T_{sep} = 0.75T_{H_1}$	1.80	0.3	1.86	0.3	WUI
$H_1 = 0.2h; H_2 = 0.4h; T_{sep} = 1.00T_{H_1}$	1.80	0.5	2.08	0.4	WUI
$H_1 = 0.3h; H_2 = 0.3h; T_{sep} = 0.75T_{H_1}$	1.00	0.3	1.35	0.3	WUI
$H_1 = 0.3h; H_2 = 0.4h; T_{sep} = 0.75T_{H_1}$	1.23	0.3	1.42	0.3	WUI
$H_1 = 0.3h; H_2 = 0.4h; T_{sep} = 1.00T_{H_1}$	1.29	0.4	1.62	0.4	WUI
$H_1 = 0.4h; H_2 = 0.3h; T_{sep} = 0.75T_{H_1}$	0.78	0.3	1.19	0.3	WUI
$H_1 = 0.4h; H_2 = 0.4h; T_{sep} = 0.75T_{H_1}$	0.97	0.2	1.24	0.3	WUI
$H_1 = 0.4h; H_2 = 0.4h; T_{sep} = 1.00T_{H_1}$	1.03	0.3	1.38	0.3	WUI
$H_1 = 0.1h; H_2 = 0.4h; T_{sep} = 1.00T_{H_1}$	3.50	0.7	3.31	0.5	WWBI
$H_1 = 0.1h; H_2 = 0.4h; T_{sep} = 1.25T_{H_1}$	3.47	0.9	3.42	0.8	WWBI
$H_1 = 0.2h; H_2 = 0.2h; T_{sep} = 0.75T_{H_1}$	1.01	0.4	1.49	0.4	WWBI
$H_1 = 0.2h; H_2 = 0.2h; T_{sep} = 1.00T_{H_1}$	1.00	0.6	1.61	0.6	WWBI
$H_1 = 0.2h; H_2 = 0.2h; T_{sep} = 1.25T_{H_1}$	1.00	0.7	1.55	0.7	WWBI
$H_1 = 0.2h; H_2 = 0.3h; T_{sep} = 1.00T_{H_1}$	1.42	0.5	1.87	0.5	WWBI
$H_1 = 0.2h; H_2 = 0.3h; T_{sep} = 1.25T_{H_1}$	1.45	0.7	1.93	0.6	WWBI
$H_1 = 0.2h; H_2 = 0.3h; T_{sep} = 1.50T_{H_1}$	1.43	0.8	1.80	0.8	WWBI
$H_1 = 0.2h; H_2 = 0.4h; T_{sep} = 1.25T_{H_1}$	1.76	0.6	2.11	0.5	WWBI
$H_1 = 0.2h; H_2 = 0.4h; T_{sep} = 1.50T_{H_1}$	1.79	0.7	2.13	0.7	WWBI
$H_1 = 0.2h; H_2 = 0.4h; T_{sep} = 1.75T_{H_1}$	1.76	0.9	1.88	0.8	WWBI
$H_1 = 0.3h; H_2 = 0.2h; T_{sep} = 0.75T_{H_1}$	0.70	0.4	1.17	0.4	WWBI
$H_1 = 0.3h; H_2 = 0.2h; T_{sep} = 1.00T_{H_1}$	0.73	0.5	1.21	0.5	WWBI
$H_1 = 0.3h; H_2 = 0.2h; T_{sep} = 1.25T_{H_1}$	0.71	0.6	1.29	0.7	WWBI
$H_1 = 0.3h; H_2 = 0.3h; T_{sep} = 1.00T_{H_1}$	1.03	0.4	1.44	0.4	WWBI
$H_1 = 0.3h; H_2 = 0.3h; T_{sep} = 1.25T_{H_1}$	1.01	0.5	1.50	0.5	WWBI
$H_1 = 0.3h; H_2 = 0.3h; T_{sep} = 1.50T_{H_1}$	1.00	0.6	1.47	0.7	WWBI
$H_1 = 0.3h; H_2 = 0.4h; T_{sep} = 1.25T_{H_1}$	1.27	0.5	1.61	0.5	WWBI
$H_1 = 0.3h; H_2 = 0.4h; T_{sep} = 1.50T_{H_1}$	1.24	0.6	1.66	0.6	WWBI
$H_1 = 0.3h; H_2 = 0.4h; T_{sep} = 1.75T_{H_1}$	1.25	0.7	1.54	0.7	WWBI
$*H_1 = 0.3h; H_2 = 0.4h; T_{sep} = 2.00T_{H_1}$	1.26	0.8	1.35	0.8	WWBI
$H_1 = 0.4h; H_2 = 0.2h; T_{sep} = 0.75T_{H_1}$	0.54	0.4	1.01	0.4	WWBI
$H_1 = 0.4h; H_2 = 0.2h; T_{sep} = 1.00T_{H_1}$	0.58	0.4	1.05	0.5	WWBI
$H_1 = 0.4h; H_2 = 0.2h; T_{sep} = 1.25T_{H_1}$	0.58	0.5	1.03	0.6	WWBI
$H_1 = 0.4h; H_2 = 0.3h; T_{sep} = 1.00T_{H_1}$	0.84	0.4	1.22	0.4	WWBI
$H_1 = 0.4h; H_2 = 0.3h; T_{sep} = 1.25T_{H_1}$	0.83	0.4	1.24	0.5	WWBI
$H_1 = 0.4h; H_2 = 0.3h; T_{sep} = 1.50T_{H_1}$	0.82	0.5	1.28	0.6	WWBI
$*H_1 = 0.4h; H_2 = 0.3h; T_{sep} = 1.75T_{H_1}$	0.79	0.6	1.07	0.7	WWBI
$H_1 = 0.4h; H_2 = 0.4h; T_{sep} = 1.25T_{H_1}$	1.03	0.4	1.35	0.4	WWBI
$H_1 = 0.4h; H_2 = 0.4h; T_{sep} = 1.50T_{H_1}$	1.03	0.5	1.42	0.5	WWBI
$H_1 = 0.4h; H_2 = 0.4h; T_{sep} = 1.75T_{H_1}$	1.00	0.6	1.32	0.6	WWBI
$*H_1 = 0.4h; H_2 = 0.4h; T_{sep} = 2.00T_{H_1}$	0.99	0.7	1.13	0.7	WWBI
$*H_1 = 0.1h; H_2 = 0.4h; T_{sep} = 1.50T_{H_1}$	3.45	1.2	1.84	1.0	SWBI

21699291, 2024, 10, Downloaded from https://agupubs.onlinelibrary.wiley.com/doi/10.1029/2024JC021126 by Nimish Pujara - University Of Wisconsin , Wiley Online Library on [14/10/2024]. See the Terms and Conditions (https://onlinelibrary.wiley.com/terms-and-conditions) on Wiley Online Library for rules of use; OA articles are governed by the applicable Creative Commons License

21699291, 2024, 10, Downloaded from https://agupubs.onlinelibrary.wiley.com/doi/10.1029/2024JC021126 by Nimish Pujara - University Of Wisconsin , Wiley Online Library on [14/10/2024]. See the Terms and Conditions (https://onlinelibrary.wiley.com/terms-and-conditions) on Wiley Online Library for rules of use; OA articles are governed by the applicable Creative Commons License

Table 1
Continued

Cases	$(H_2/H_1)_{CP_1}$	$(T_{sep}/T_{swash})_{CP_1}$	$(H_2/H_1)_{CP_2}$	$(T_{sep}/T_{swash})_{CP_2}$	Type
$H_1 = 0.2h; H_2 = 0.2h; T_{sep} = 1.50T_{H_1}$	0.99	0.9	1.51	0.9	SWBI
$H_1 = 0.2h; H_2 = 0.2h; T_{sep} = 1.75T_{H_1}$	1.00	1.0	0.66	1.1	SWBI
$H_1 = 0.2h; H_2 = 0.2h; T_{sep} = 2.00T_{H_1}$	1.00	1.1	0.56	1.2	SWBI
$*H_1 = 0.2h; H_2 = 0.3h; T_{sep} = 1.75T_{H_1}$	1.40	0.9	1.71	0.9	SWBI
$*H_1 = 0.2h; H_2 = 0.3h; T_{sep} = 2.00T_{H_1}$	1.43	1.1	0.74	1.1	SWBI
$*H_1 = 0.2h; H_2 = 0.4h; T_{sep} = 2.00T_{H_1}$	1.81	1.0	1.30	1.0	SWBI
$*H_1 = 0.3h; H_2 = 0.2h; T_{sep} = 1.50T_{H_1}$	0.69	0.7	0.97	0.8	SWBI
$*H_1 = 0.3h; H_2 = 0.2h; T_{sep} = 1.75T_{H_1}$	0.71	0.8	0.86	0.9	SWBI
$H_1 = 0.3h; H_2 = 0.2h; T_{sep} = 2.00T_{H_1}$	0.70	0.9	0.64	1.0	SWBI
$*H_1 = 0.3h; H_2 = 0.3h; T_{sep} = 1.75T_{H_1}$	1.01	0.7	1.32	0.8	SWBI
$*H_1 = 0.3h; H_2 = 0.3h; T_{sep} = 2.00T_{H_1}$	1.00	0.8	1.39	0.9	SWBI
$H_1 = 0.4h; H_2 = 0.2h; T_{sep} = 1.50T_{H_1}$	0.56	0.6	0.83	0.7	SWBI
$H_1 = 0.4h; H_2 = 0.2h; T_{sep} = 1.75T_{H_1}$	0.56	0.7	0.90	0.8	SWBI
$H_1 = 0.4h; H_2 = 0.2h; T_{sep} = 2.00T_{H_1}$	0.56	0.8	0.88	0.9	SWBI
$*H_1 = 0.4h; H_2 = 0.3h; T_{sep} = 2.00T_{H_1}$	0.79	0.7	0.90	0.8	SWBI
$H_1 = 0.1h; H_2 = 0.4h; T_{sep} = 1.75T_{H_1}$	3.52	1.4	1.84	1.2	No Interaction
$H_1 = 0.1h; H_2 = 0.4h; T_{sep} = 2.00T_{H_1}$	3.58	1.6	2.33	1.4	No Interaction

Note. The interaction types include wave-uprush interaction (WUI), weak wave-backwash interaction (WWBI), and strong wave-backwash interaction (SWBI). Cases marked with * were not analyzed, as explained in the main text.

3. Results

3.1. Single Solitary Wave

We use the results of single solitary wave experiments to extract information of single swash events that can be used as a baseline to understand the wave-swash events driven by consecutive solitary waves. Figure 2 shows data of the wave period measured at different cross-shore locations for single solitary wave experiments. At CP_1, beach toe, and CP_2, the wave period is estimated as the time over which the free-surface displacement timeseries is above a small threshold (2.5 mm for $H/h = [0.1, 0.2, 0.3]$ and 4 mm for $H/h = 0.4$ where the larger threshold for the larger amplitude wave captures a representative period associated with this steeper wave). The 'effective period' is taken from the widely used definition the period for a solitary wave in Madsen et al. (2008) (their Equation 6) using the wave amplitude at CP_1. In the constant depth region, beach toe, and at CP_2, the period decreases with increasing wave height. This decrease can be understood in terms of the mechanics of solitary waves, where the wave height and the wavelength are linked. In particular, it is well known that solitary waves become narrower as the wave height increases (Madsen et al., 2008).

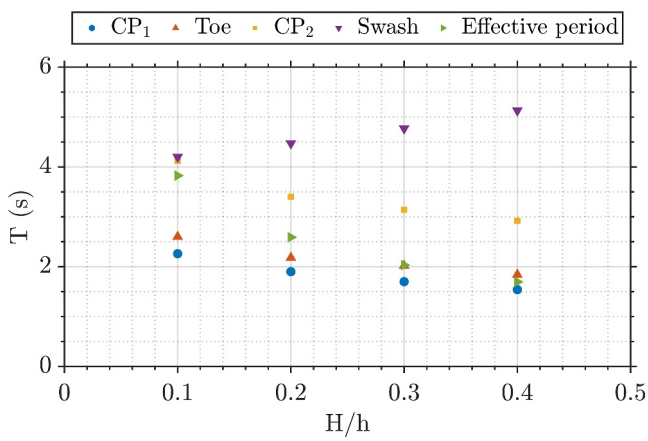

Figure 2. Wave or swash period measured at different locations along the flume.

These results of decreasing wave period with increasing wave height are counter intuitive for the swash event. We expected, and observed, that waves of larger wave height generated larger swash events that reached a higher run-up and took longer to complete the uprush-backwash swash cycle. Thus, it is clear that the wave periods measured offshore of the SWL do not provide a good measure of the period of the swash event. To estimate the true swash period, we used the camera images to find the time between when the shoreline at the still water line first begins to move during the uprush to when a hydraulic jump begins to form during the downrush. This definition of the

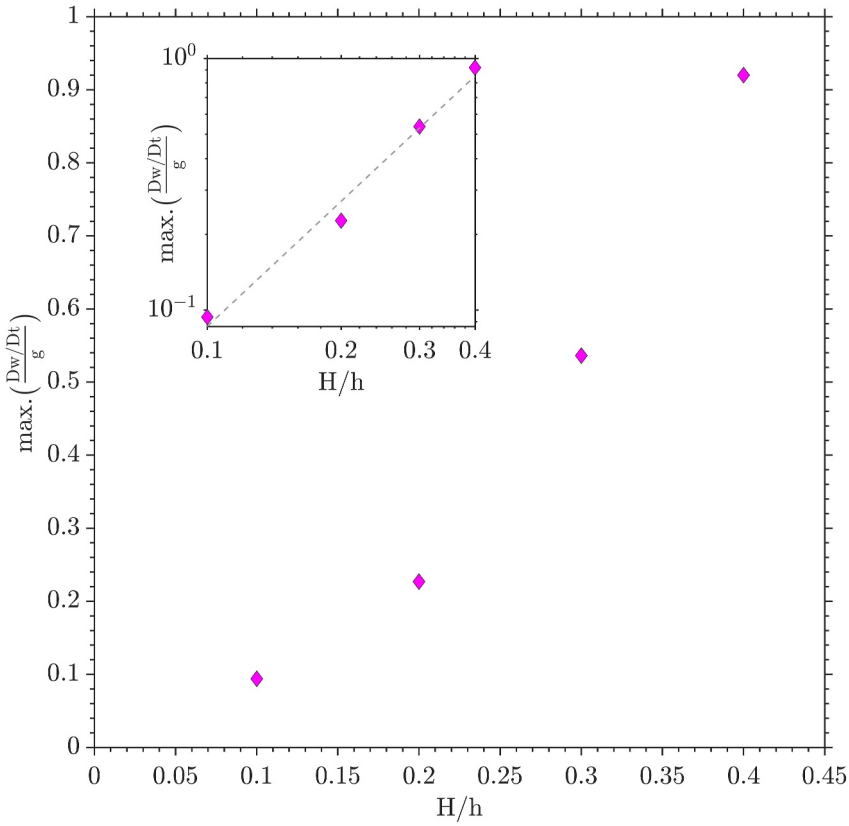

Figure 3. Peak upward-directed vertical accelerations at CP_2 as a function of incident solitary wave height. Inset shows the same data with the best-fit power law exponent of 1.65.

swash period, which is consistent with previous work (Pujara et al., 2015a), allows us to understand the influence of wave-swash interactions. Sudden changes in water depth and flow velocities are attributed to wave-swash interactions only if a subsequent wave front arrives before the end of the swash period; otherwise, they may be due to the backwash hydraulic jump. The swash period is shown in Figure 2 and supports basic intuition and observations: the swash period increases with incident wave height. This result also underscores the importance of measuring the swash period directly. In the analysis of wave-swash interactions presented below, we emphasize the importance of this swash period, T_{swash}. In particular, the quantity T_{sep}/T_{swash} is the dynamically important dimensionless separation time between consecutive swash events.

Figure 3 shows the upward-directed peak vertical accelerations measured at CP_2 (as described in Section 2.3) for single solitary wave experiments as a function of wave height. These peak vertical accelerations occur before the wave crest during the passage of the wave front. As wave height increases, we observe larger vertical accelerations with values close to gravity for the largest wave tested. The Boussinesq (1872) theory of solitary waves allows us to predict how the maximum vertical acceleration varies with the wave height in the constant depth region. Using the Boussinesq solution for the fluid velocities in a solitary wave (Equation 2.2 in Pujara et al. (2015a)), it is easily shown that the peak vertical acceleration follows $Dw/Dt \sim (H/h)^{3/2}$ to leading order and that this scaling comes from the local time derivative ($\partial w/\partial t$) which dominates over the advective acceleration ($\mathbf{u} \cdot \nabla w$).

The inset in Figure 3 shows that the peak vertical acceleration at CP_2 follows a power law with a power-law exponent that is empirically found to be 1.65. The similarity of this value with the predicted value of 1.5 using solitary wave theory in constant depth suggests the peak vertical accelerations for wave crests during their climb of a sloping beach can be understood in terms of incident wave properties, even up to very shallow water depths where the wave shape has evolved significantly during shoaling. It also suggests that shoaling of a wave crest in otherwise quiescent water is insufficient to generate vertical accelerations that exceed gravity.

21699291, 2024, 10, Downloaded from https://agupubs.onlinelibrary.wiley.com/doi/10.1029/2024JC021126 by Nimish Pujara - University Of Wisconsin , Wiley Online Library on [14/10/2024]. See the Terms and Conditions (https://onlinelibrary.wiley.com/terms-and-conditions) on Wiley Online Library for rules of use; OA articles are governed by the applicable Creative Commons License

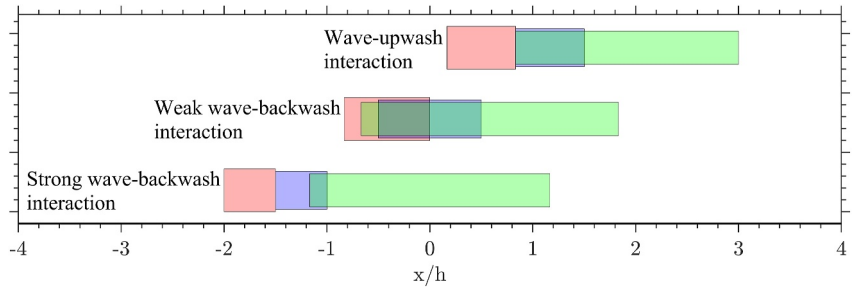

Figure 4. Spatial extent of wave-swash interactions and their different stages: jet slamming (red), splash-induced flow (purple), and fully 3D turbulent flow (green). Wave-upwash interaction ($H_1 = 0.2h$; $H_2 = 0.4h$; $T_{sep} = 1.0T_{H_1}$); weak wave-backwash interaction ($H_1 = 0.3h$; $H_2 = 0.3h$; $T_{sep} = 1.5T_{H_1}$); and strong wave-backwash interaction ($H_1 = 0.3h$; $H_2 = 0.2h$; $T_{sep} = 1.5T_{H_1}$).

3.2. Consecutive Solitary Waves

3.2.1. Wave-Swash Interaction Types and Interaction Zones

Figure 4 maps out the typical stages of a wave-swash interaction with examples of each interaction type. From the camera images, we observed that wave-swash interactions consistently displayed three stages: First, the overturning crest of the second wave created a jet which struck the water ahead of it ("jet slamming"). Second, this breaker jet created a splash that altered the shallow flow ahead of the breaker ("splash-induced flow"). Finally, this interaction between the breaker and the swash of the preceding wave showed signs of fluid instabilities that quickly transitioned into highly turbulent flow ("fully 3D turbulent flow"). Some aspects of these observations have also been reported in the inner surf and swash zones of plunging breaker regular waves (Sou & Yeh, 2011; Sumer et al., 2013). However, the location of where the interaction takes place, as well as the spatial extent where these three stages occur, varies for different wave-swash interaction types, which has not been previously reported in laboratory studies. As Figure 4 shows, the interaction zone moves offshore for wave-backwash interactions compared with wave-uprush interactions and there is less overlap in the spatial extent of the three stages for strong wave-backwash interactions compared with weak wave-backwash interactions.

3.2.2. Hydrodynamics of Wave-Swash Interactions

While the qualitative wave-swash interaction types and stages described above are useful for classification purposes, they do not reveal any information of the underlying hydrodynamics. Thus, we now tackle the quantitative analysis of wave-swash interactions. Figures 5–7 show the typical timeseries at CP_2 for wave-upwash, weak wave-backwash, and strong wave-backwash interactions, respectively. Gaps in the data are related to quality control procedures described in Section 2.1. In the bed pressure data, there are large fluctuations after the passage of the first wave crest. These are associated with beach vibrations induced by the jet slamming of the first wave and are therefore experimental artifacts.

The top panels in Figures 5–7 show the total water depth and bed pressure in units of depth together, which when compared with the vertical accelerations in the middle panel, show how the vertical accelerations result from a non-hydrostatic pressure distribution. Focusing on the vertical accelerations, it is evident that the passage of a shoaling wave crest into quiescent water generates accelerations of magnitude up to that of gravity, whereas the a wave crest interacting with the swash event of the previous wave results in larger acceleration with values far exceeding gravity. The velocity data in the bottom panel shows that the peak vertical acceleration in the wave-swash interaction is near concurrent with the peak positive horizontal and vertical velocities. Though we do not show it explicitly, the velocity data also show that, in contrast to single solitary wave data, the local time derivative of the vertical velocity ($\partial w/\partial t$) is insufficient to explain the inferred vertical accelerations, suggesting that the advective part of the vertical acceleration ($\mathbf{u} \cdot \nabla w$) is important. Finally, we note that the qualitative wave-swash interaction types do not necessarily predict the hydrodynamics, but the advantage of our experimental setup is that the wave height ratio H_2/H_1 and the dimensionless separation time T_{sep}/T_{swash} provide a quantitative parameter space in which we can map out the hydrodynamics.

21699291, 2024, 10, Downloaded from https://agupubs.onlinelibrary.wiley.com/doi/10.1029/2024JC021126 by Nimish Pujara - University Of Wisconsin , Wiley Online Library on [14/10/2024]. See the Terms and Conditions (https://onlinelibrary.wiley.com/terms-and-conditions) on Wiley Online Library for rules of use; OA articles are governed by the applicable Creative Commons License

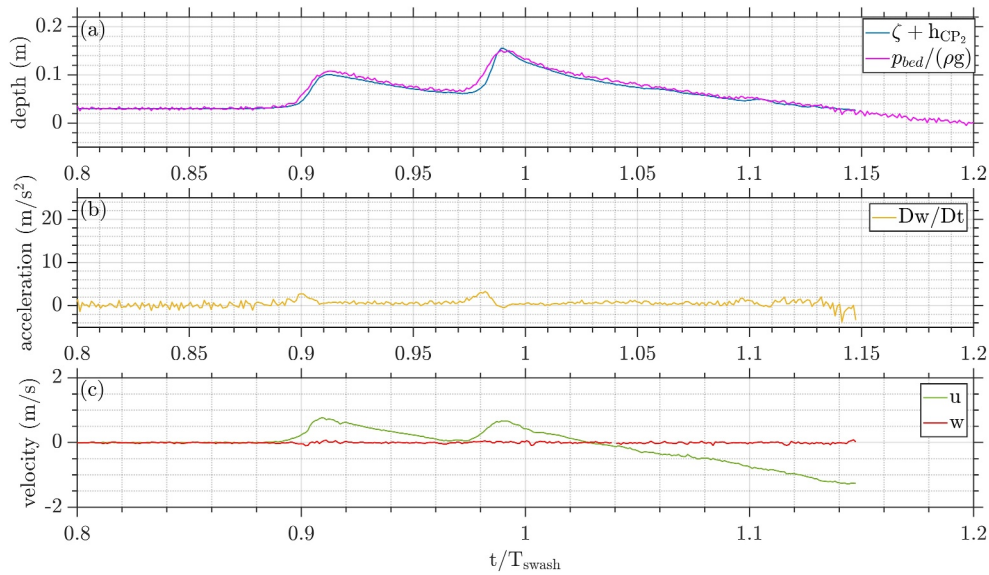

Figure 5. Time series of depth, bottom pressure converted to depth, velocity, and estimated total vertical acceleration for a wave-upwash interaction case: $H_1 = 0.2h$; $H_2 = 0.3h$; $T_{sep} = 0.75T_{H_1}$ ($H_2/H_1 = 1.5$, $T_{sep} = 0.084T_{swash}$).

Figure 8 shows the distribution of the wave-swash interactions as a function of H_2/H_1 and T_{sep}/T_{swash} as measured at CP_1 (upper left panel) and CP_2 (upper right panel). Satisfyingly, the observed qualitative interaction types cluster together based on the incident wave information at CP_1: Wave-uprush interactions are in the bottom-right region, weak wave-backwash interactions are in the middle, and strong wave-backwash interactions are in the top-left region. Quantitative thresholds have been provided to delimit the regions for the different interaction groups for the data at CP_1, with clear trends for the different interactions. The differences between the panels, which are driven by the location where the wave heights and separation time are measured, are also instructive (bottom panel). From CP_1 ("far field") to CP_2 ("local"), the clusters of different interaction types become even more distinct from each other. At CP_2, the interactions are almost exclusively of the strong wave-backwash type for values of $H_2/H_1 < 1$ and the wave-uprush and weak wave-backwash interactions are separated only by the

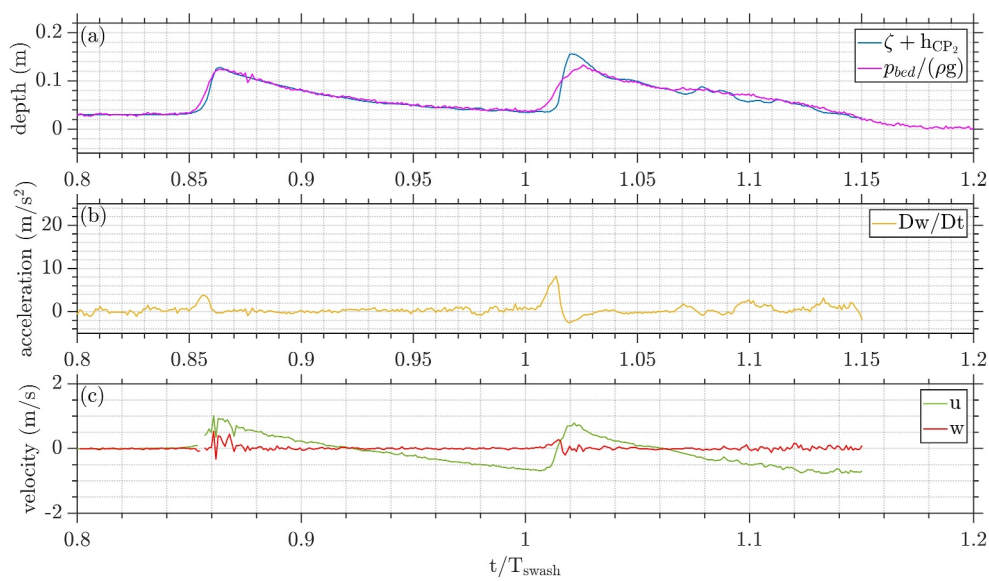

Figure 6. Time series of depth, bottom pressure converted to depth, velocity, and estimated total vertical acceleration for a weak wave-backwash interaction case: $H_1 = 0.3h$; $H_2 = 0.2h$; $T_{sep} = 1.25T_{H_1}$ ($H_2/H_1 = 0.667$, $T_{sep} = 0.128T_{swash}$).

21699291, 2024, 10, Downloaded from https://agupubs.onlinelibrary.wiley.com/doi/10.1029/2024JC021126 by Nimish Pujara - University Of Wisconsin , Wiley Online Library on [14/10/2024]. See the Terms and Conditions (https://onlinelibrary.wiley.com/terms-and-conditions) on Wiley Online Library for rules of use; OA articles are governed by the applicable Creative Commons License

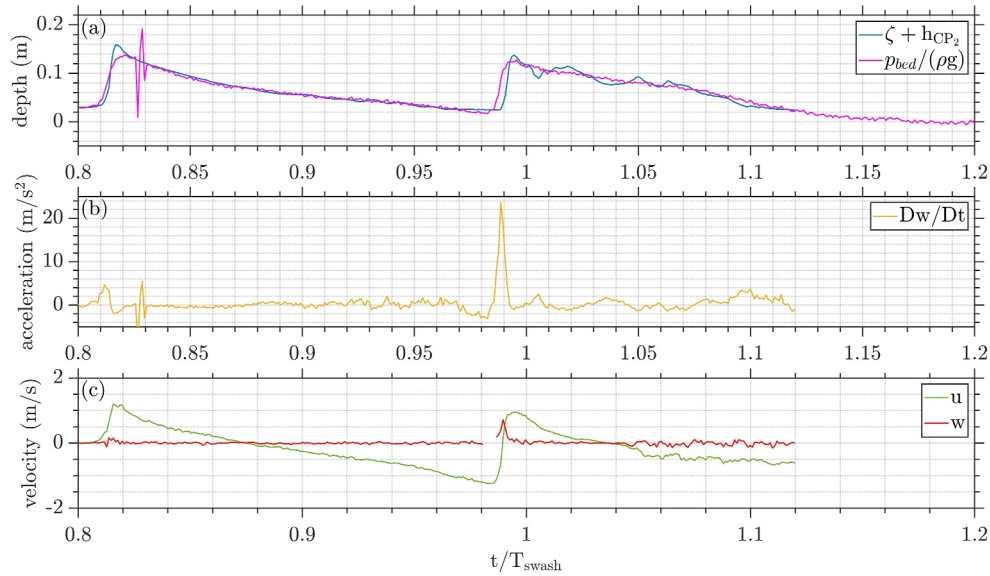

Figure 7. Time series of depth, bottom pressure converted to depth, velocity, and estimated total vertical acceleration for a strong wave-backwash interaction case: $H_1 = 0.4h$; $H_2 = 0.2h$; $T_{sep} = 1.50T_{H_1}$ ($H_2/H_1 = 0.5$, $T_{sep} = 0.137T_{swash}$).

T_{sep}/T_{swash} for values of $H_2/H_1 > 1$. Since our main interest is in understanding the flow and accelerations in the wave-swash interaction zone, the following analyses will focus on measurements from CP_2.

Figure 9 presents the main results of this study: the peak upward-directed vertical acceleration magnitude as a function of H_2/H_1 and T_{sep}/T_{swash} at CP_2. We observe that while the peak accelerations are larger for wave-backwash interactions (whether weak or strong) compared with wave-uprush interactions, it is not necessarily the case that strong wave-backwash interactions produce larger accelerations than weak wave-backwash interactions. The data show that there is a region of the parameter space, approximately $0.5 < H_2/H_1 < 2$ and $0.6 < T_{sep}/T_{swash} < 1.2$, where the peak accelerations are the largest. Physically, this corresponds to situations where the strength of the backwash flows generated by the swash of the first wave collide with an incoming wave front with approximately equal and opposite velocities. The peak vertical acceleration in the interaction is not particularly large if the velocity in either the backwash of the first wave or the wave front of the second wave dominates over the other.

In Figure 10, we investigate the time at which the peak vertical acceleration, T_{peak}, occurs during the wave-swash interaction. This is to understand how it relates to the swash period T_{swash} and the magnitude of the acceleration peak. The timing of the peak is not necessarily solely dependent on T_{sep} (left panel), but the largest peak accelerations occur during the later stages of the swash flow associated with the first wave ($T_{peak}/T_{swash} \approx 1$) (right panel).

The final analysis relates to the correlations between the peak vertical accelerations and the flow velocities. Since our interest in vertical accelerations stems from the possibility of inducing large material suspension events, it is important to consider the direction and magnitude of the flow velocity at the same time since that will influence the speed and direction in which suspended material is advected. Figure 11 shows the velocity extracted at the time of peak vertical accelerations. The correlation between the peak vertical acceleration and the horizontal velocity is very weak, but interestingly, the vertical velocity at the time of peak vertical acceleration shows a (weak) positive correlation, suggesting that if large vertical accelerations destabilize a sediment bed or flush pore water with dissolved materials out of the bed, the flow field would act to transport that material upwards into the water column.

While the fluid velocity at the time of the vertical acceleration peak is important, the timeseries data in Figures 5–7 also show that the peak positive horizontal and vertical velocities occur either shortly before or shortly after the peak acceleration. To quantify this, we calculate the time lag between the peak upward vertical acceleration and the peak positive fluid velocity for both components in Figure 12. Positive values indicate that the peak positive

21699291, 2024, 10, Downloaded from https://agupubs.onlinelibrary.wiley.com/doi/10.1029/2024JC021126 by Nimish Pujara - University Of Wisconsin , Wiley Online Library on [14/10/2024]. See the Terms and Conditions (https://onlinelibrary.wiley.com/terms-and-conditions) on Wiley Online Library for rules of use; OA articles are governed by the applicable Creative Commons License

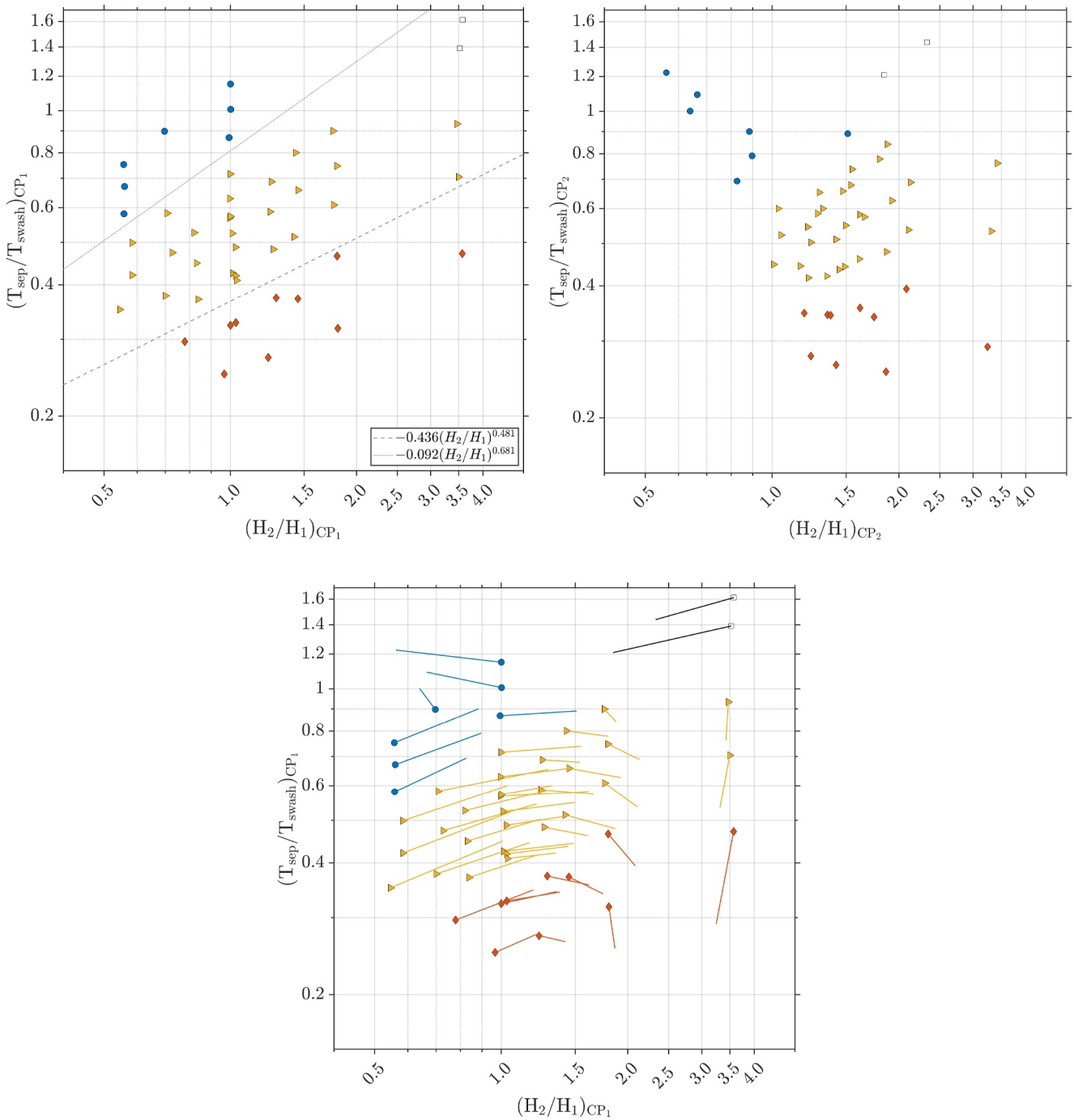

Figure 8. Wave-swash interaction types as functions of H_2/H_1 and T_{sep}/T_{swash}. Measurements at CP_1 (upper left panel); measurements at CP_2 (upper left panel); and transition of the interactions from CP_1 to CP_2 (bottom panel). Wave-uprush interaction (diamonds), weak wave-backwash interaction (triangles), strong wave-backwash interaction (circles), no interaction (blank squares).

velocity precedes the peak positive acceleration whereas negative values indicate that the peak acceleration precedes the peak velocity. The results show that in most cases, the peak vertical acceleration precedes the peak positive (onshore directed) horizontal velocity, suggesting that even if there is not a strong correlation between the horizontal velocity and the vertical acceleration at the moment when the peak acceleration occurs, any material suspended into the water column by the vertical dynamics is prone to be transported onshore shortly after by the horizontal flow.

21699291, 2024, 10, Downloaded from https://agupubs.onlinelibrary.wiley.com/doi/10.1029/2024JC021126 by Nimish Pujara - University Of Wisconsin , Wiley Online Library on [14/10/2024]. See the Terms and Conditions (https://onlinelibrary.wiley.com/terms-and-conditions) on Wiley Online Library for rules of use; OA articles are governed by the applicable Creative Commons License

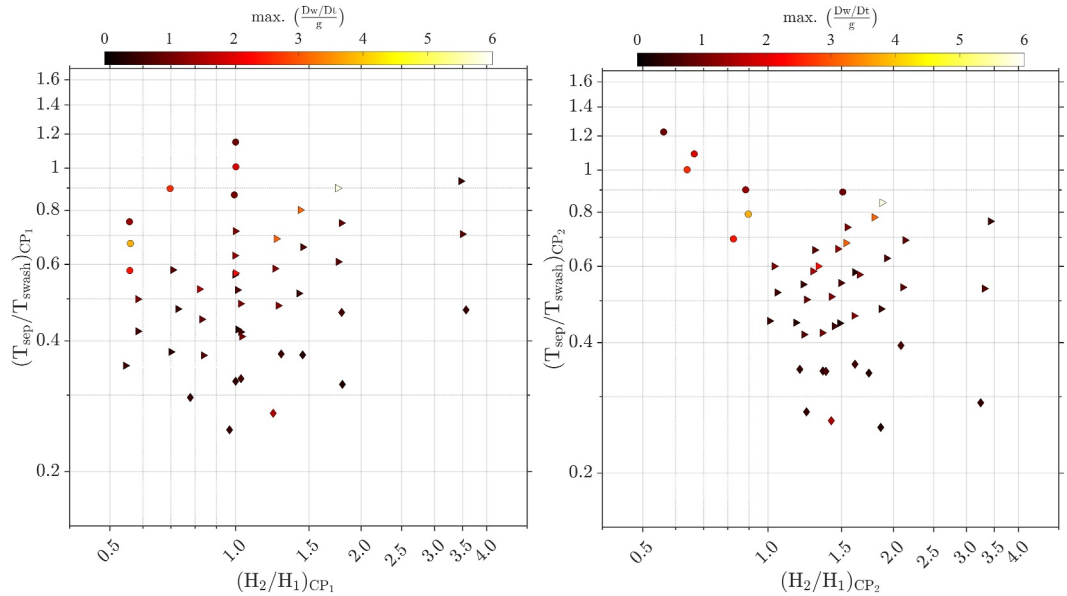

Figure 9. Peak total vertical accelerations as functions of H_2/H_1 and T_{sep}/T_{swash}. Measurements at CP_1 (left). Measurements at CP_2 (right). Wave-upwash interaction (diamonds), weak wave-backwash interaction (triangles), strong wave-backwash interaction (circles).

4. Discussion

We have found that different qualitative wave-swash interaction types (i.e., wave-uprush interactions, weak wave-backwash interactions, and strong wave-backwash interactions) form distinct clusters in the dimensionless space mapped by the ratio of consecutive wave heights (H_2/H_1) and the time separation between wave crests made dimensionless by the swash period of the first wave (T_{sep}/T_{swash}). While this finding is based on measurements at a constant beach slope which limits the range of wave breaker types, the same dimensionless parameters are expected to be sufficient to predict wave-swash interactions on different beach slopes. This is

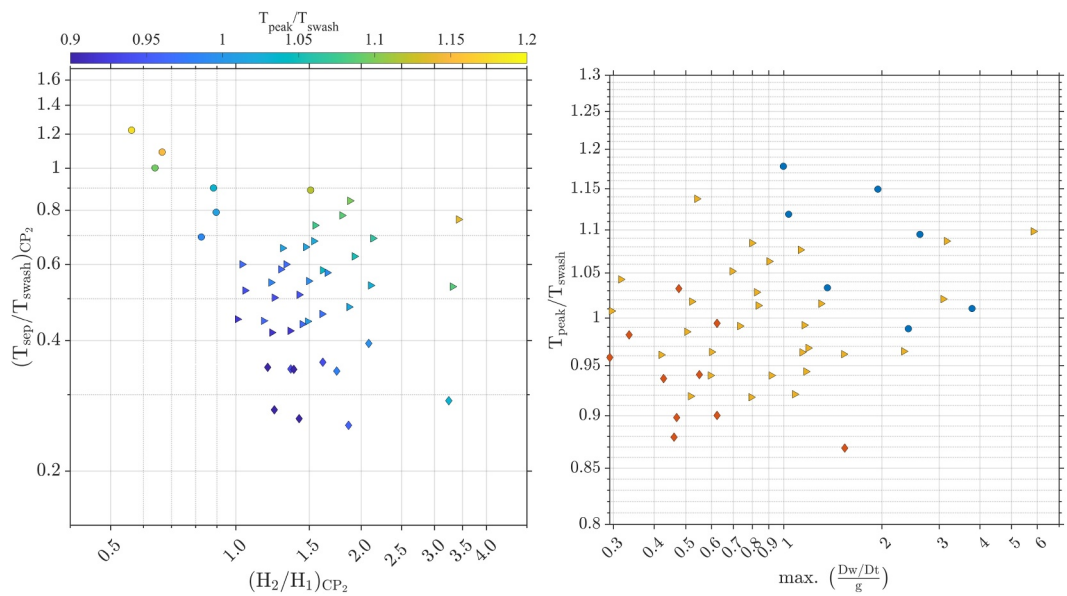

Figure 10. Time of peak total vertical acceleration as functions of H_2/H_1 and T_{sep}/T_{swash} (left). Peak vertical accelerations as a function of time of peak vertical acceleration (right). Wave-upwash interaction (diamonds), weak wave-backwash interaction (triangles), strong wave-backwash interaction (circles).

21699291, 2024, 10, Downloaded from https://agupubs.onlinelibrary.wiley.com/doi/10.1029/2024JC021126 by Nimish Pujara - University Of Wisconsin , Wiley Online Library on [14/10/2024]. See the Terms and Conditions (https://onlinelibrary.wiley.com/terms-and-conditions) on Wiley Online Library for rules of use; OA articles are governed by the applicable Creative Commons License

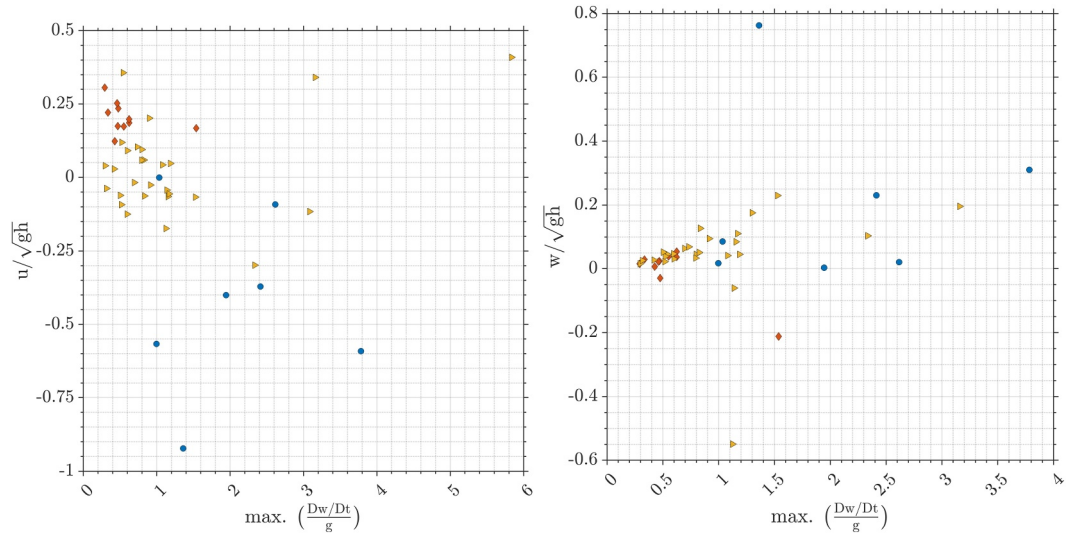

Figure 11. Correlations between the peak total vertical accelerations and fluid velocities. Horizontal velocity component (left) and vertical velocity component (right). Wave-upwash interaction (diamonds), weak wave-backwash interaction (triangles), strong wave-backwash interaction (circles).

because they include all the variables that control how the swash created by a wave affects the subsequent wave, with the beach slope only altering the wave breaker types and run-ups (see, e.g., Barale et al. (2024) who show data of consecutive dam-breaks over multiple beach slopes). The influence of wave breaker types on swash flow occurs through how the bore collapse process is modified and does not fundamentally alter the nature of the swash flow (Pujara et al., 2015a; Yeh & Ghazali, 1988).

The main focus of the study was on the vertical accelerations, which were estimated from the differences between the depth measured with a surface wave gauge and the depth inferred from pressure measurements at the bed

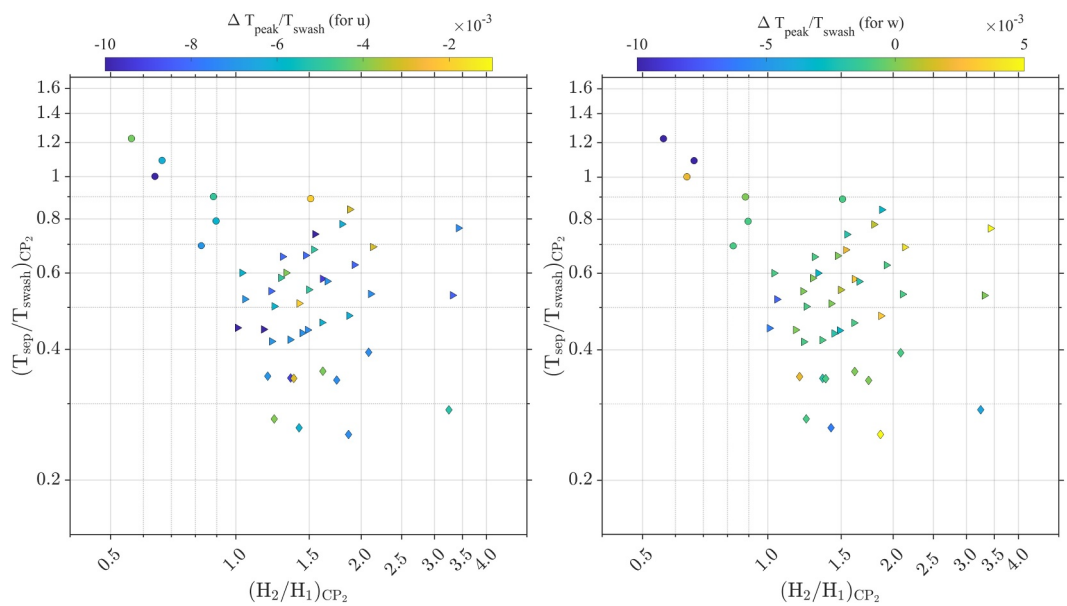

Figure 12. Time lag between the peak total vertical acceleration and maximum velocities as functions of H_2/H_1 and T_{sep}/T_{swash}. Positive values indicate that the peak positive velocity precedes the peak positive acceleration whereas negative values indicate that the peak acceleration precedes the peak velocity. Horizontal velocity component (left) and vertical velocity component (right). Wave-upwash interaction (diamonds), weak wave-backwash interaction (triangles), strong wave-backwash interaction (circles).

21699291, 2024, 10, Downloaded from https://agupubs.onlinelibrary.wiley.com/doi/10.1029/2024JC021126 by Nimish Pujara - University Of Wisconsin , Wiley Online Library on [14/10/2024]. See the Terms and Conditions (https://onlinelibrary.wiley.com/terms-and-conditions) on Wiley Online Library for rules of use; OA articles are governed by the applicable Creative Commons License

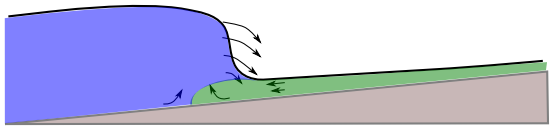

Figure 13. Sketch of the mechanism by which wave-swash interactions lead to large vertical accelerations. The green region shows the backwash flow of the first wave and the blue region shows the incoming bore of the second wave. The collision of the fast backwash flow with the steep bore front redirects flow upwards with a larger vertical acceleration.

under the assumption that the viscous and turbulent Reynolds stresses are small enough to neglect. The largest vertical accelerations were associated with wave-swash interactions that spanned $0.5 < H_2/H_1 < 2$ and $0.6 < T_{sep}/T_{swash} < 1.2$, where the vertical accelerations commonly exceeded gravity. These wave-swash interactions corresponded to cases where the separation time, T_{sep}, is comparable to the swash time for the preceding wave, T_{swash}, which allows for the development of a strong backwash flow in the first wave that interacts with the collapse of the second incoming wave. This mechanism is sketched in Figure 13. The large vertical accelerations are important for nearshore transport processes; it suggests that wave-swash interactions may be an effective mechanism by which material such as sediment or solutes within sediment pores is suspended into the water column before being advected in the cross-shore direction. In particular, it could be the cause of the local momentary liquefaction observed in field studies (Florence et al., 2022; Marry & Foster, 2024) or the cause of large sediment suspension events observed in lab studies (Alsina et al., 2018; Park, 2009). However, turbulent Reynolds stresses may also play role in these processes, and their importance remains to be investigated using numerical modeling or detailed velocity measurements.

The data in this study are limited to a single location within the swash zone, but the results demonstrate the need to make detailed measurements of the flow and accelerations throughout the swash zone for wave-swash interactions in future studies to understand their impact on transport processes. In particular, non-hydrostatic effects are likely to be important in wave-swash interactions even if they are not important in a single swash event. We show that the qualitative wave-swash interaction type can be predicted from knowledge of incident waves using the dimensionless ratios mentioned above, but that knowing only the interaction type is insufficient to predict the flow and accelerations.

5. Concluding Remarks

In a set of controlled laboratory experiments, we used solitary waves to generate isolated swash events and successive solitary waves to generate isolated wave-swash interaction events. Through independent control of the wave heights and the time separation between them, it was possible to reproduce the range of wave-swash interactions found in the field, such as wave-upwash, weak wave-backwash, and strong wave-backwash interactions. We found that the wave-swash interaction types can be predicted based on information of the incident waves via two dimensionless ratios: (a) the ratio of consecutive wave heights (H_2/H_1) and (b) the time separation between successive wave crests made dimensionless by the swash period of the first wave (T_{sep}/T_{swash}). Our focus was on quantifying the flow and vertical accelerations in wave-swash interactions, and our findings show that non-hydrostatic pressure distributions, which are typically ignored in modeling coastal flows in the very shallow waters of the inner-surf and swash zones, can generate large vertical accelerations that could lead to the suspension of sediment and solutes within sediment pores.

Data Availability Statement

The measured data, corresponding to time series of velocities, bottom pressures, and surface elevations used for the analyses of flows and accelerations induced by wave-swash are available through GitHub-Zenodo via https://doi.org/10.5281/zenodo.12699740 (Meza-Valle, 2024). Version 1.0 of the MATLAB scripts used for the analyses and graphics generated in this work is preserved on GitHub and accessed through GitHub-Zenodo (https://doi.org/10.5281/zenodo.12699740) (Meza-Valle, 2024). Data and codes are available via GNU General Public License v3.

Acknowledgments
We gratefully acknowledge funding from the US National Science Foundation (OCE-2048676). NP acknowledges an Early-Career Research Fellowship from the Gulf Research Program of the National Academies of Sciences, Engineering, and Medicine. CMV acknowledges support from the UW-Madison Graduate School and help from WSEL lab manager James Lazarcik in experimental setup.

References

Alsina, J. M., cáceres, I., Brocchini, M., & Baldock, T. (2012). An experimental study on sediment transport and bed evolution under different swash zone morphological conditions. *Coastal Engineering*, *68*, 31–43. https://doi.org/10.1016/j.coastaleng.2012.04.008

Alsina, J. M., Falchetti, S., & Baldock, T. E. (2009). Measurements and modelling of the advection of suspended sediment in the swash zone by solitary waves. *Coastal Engineering*, *56*(5–6), 621–631. https://doi.org/10.1016/j.coastaleng.2009.01.007

Alsina, J. M., Padilla, E. M., & Cáceres, I. (2016). Sediment transport and beach profile evolution induced by bi-chromatic wave groups with different group periods. *Coastal Engineering*, *114*, 325–340. https://doi.org/10.1016/j.coastaleng.2016.04.020

Alsina, J. M., van der Zanden, J., Cáceres, I., & Ribberink, J. S. (2018). The influence of wave groups and wave-swash interactions on sediment transport and bed evolution in the swash zone. *Coastal Engineering*, *140*, 23–42. https://doi.org/10.1016/j.coastaleng.2018.06.005

21699291, 2024, 10, Downloaded from https://agupubs.onlinelibrary.wiley.com/doi/10.1029/2024JC021126 by Nimish Pujara - University Of Wisconsin , Wiley Online Library on [14/10/2024]. See the Terms and Conditions (https://onlinelibrary.wiley.com/terms-and-conditions) on Wiley Online Library for rules of use; OA articles are governed by the applicable Creative Commons License

Baldock, T. E., & Holmes, P. (1999). Simulation and prediction of swash oscillations on a steep beach. *Coastal Engineering*, *36*(3), 219–242. https://doi.org/10.1016/S0378-3839(99)00011-3

Barale, J., Lacaze, L., Astruc, D., Almar, R., & Almeida, L. P. (2024). Model of bores interaction in the swash. *Coastal Engineering*, *104564*, 104564. https://doi.org/10.1016/j.coastaleng.2024.104564

Barranco, I., & Liu, P. L.-F. (2021). Run-up and inundation generated by non-decaying dam-break bores on a planar beach. *Journal of Fluid Mechanics*, *915*(A81), 1–29. https://doi.org/10.1017/jfm.2021.98

Boussinesq, J. (1872). Théorie des ondes et des remous qui se propagent le long d'un canal rectangulaire horizontal, en communiquant au liquide contenu dans ce canal des vitesses sensiblement pareilles de la surface au fond. *Journal de Mathematiques Pures et Appliquees*, *17*, 55–108. Retrieved from https://api.semanticscholar.org/CorpusID:125469048

Brocchini, M., & Baldock, T. E. (2008). Recent advances in modeling swash zone dynamics: Influence of surf-swash interaction on nearshore hydrodynamics and morphodynamics. *Reviews of Geophysics*, *46*(3), RG3003. https://doi.org/10.1029/2006RG000215

Chardón-Maldonado, P., Pintado-Patiño, J. C., & Puleo, J. A. (2016). Advances in swash-zone research: Small-scale hydrodynamic and sediment transport processes. *Coastal Engineering*, *115*, 8–25. https://doi.org/10.1016/j.coastaleng.2015.10.008

Chen, B.-T., Kikkert, G. A., Pokrajac, D., & Dai, H.-J. (2016). Experimental study of bore-driven swash–swash interactions on an impermeable rough slope. *Coastal Engineering*, *108*, 10–24. https://doi.org/10.1016/j.coastaleng.2015.10.010

Chen, W., van der Werf, J. J., & Hulscher, S. J. M. H. (2023). A review of practical models of sand transport in the swash zone. *Earth-Science Reviews*, *238*, 104355. https://doi.org/10.1016/j.earscirev.2023.104355

Dean, R. G., & Dalrymple, R. A. (2004). *Coastal processes with engineering applications*. Cambridge University Press. Retrieved from https://api.semanticscholar.org/CorpusID:59132061

Elfrink, B., & Baldock, T. (2002). Hydrodynamics and sediment transport in the swash zone: A review and perspectives. *Coastal Engineering*, *45*(3–4), 149–167. https://doi.org/10.1016/S0378-3839(02)00032-7

Erikson, L., Larson, M., & Hanson, H. (2005). Prediction of swash motion and run-up including the effects of swash interaction. *Coastal Engineering*, *52*(3), 285–302. https://doi.org/10.1016/j.coastaleng.2004.12.001

Florence, M., Stark, N., Raubenheimer, B., & Elgar, S. (2022). Nearshore vertical pore pressure gradients and onshore sediment transport under tropical storm forcing. *Journal of Waterway, Port, Coastal, and Ocean Engineering*, *148*(6), 04022023. https://doi.org/10.1061/(ASCE)WW.1943-5460.0000723

Goring, D. G. (1979). *Tsunamis–the propagation of long waves onto a shelf* Doctoral Thesis. California Institute of Technology. Retrieved from https://api.semanticscholar.org/CorpusID:117755717

Holthuijsen, L. H. (2007). *Waves in oceanic and coastal waters*. Cambridge University Press. https://doi.org/10.1017/CBO9780511618536

Hughes, M. G., & Moseley, A. S. (2007). Hydrokinematic regions within the swash zone. *Continental Shelf Research*, *27*(15), 2000–2013. https://doi.org/10.1016/j.csr.2007.04.005

Jackson, D. W. T., & Short, A. D. (2020). *Sandy beach morphodynamics*. Elsevier. https://doi.org/10.1016/C2018-0-02420-2

Kikkert, G. A., O'Donoghue, T., Pokrajac, D., & Dodd, N. (2012). Experimental study of bore-driven swash hydrodynamics on impermeable rough slopes. *Coastal Engineering*, *60*, 149–166. https://doi.org/10.1016/j.coastaleng.2011.09.006

Liu, P. L.-F., Park, Y. S., & Cowen, E. A. (2007). Boundary layer flow and bed shear stress under a solitary wave. *Journal of Fluid Mechanics*, *574*, 449–463. https://doi.org/10.1017/jfm.2014.52

Lo, H.-Y., Park, Y. S., & Liu, P. L.-F. (2013). On the run-up and back-wash processes of single and double solitary waves—An experimental study. *Coastal Engineering*, *80*, 1–14. https://doi.org/10.1016/j.coastaleng.2013.05.001

Madsen, P. A., Fuhrman, D. R., & Schäffer, H. A. (2008). On the solitary wave paradigm for tsunamis. *Journal of Geophysical Research*, *113*(C12), C12012. https://doi.org/10.1029/2008JC004932

Mancini, G., Briganti, R., McCall, R., Dodd, N., & Zhu, F. (2021). Numerical modelling of intra-wave sediment transport on sandy beaches using a non-hydrostatic, wave-resolving model. *Ocean Dynamics*, *71*(1), 1–20. https://doi.org/10.1007/s10236-020-01416-x

Marry, M., & Foster, D. (2024). Field observations of hydrostatic pressure deviations in a nearshore sediment bed. *Journal of Geophysical Research: Oceans*, *129*(2), 1–21. https://doi.org/10.1029/2023JC019891

Martínez, C., Contreras-Lopez, M., Winckler, P., Hidalgo, H., Godoy, E., & Agredano, R. (2018). Coastal erosion in central Chile: A new hazard? *Ocean & Coastal Management*, *156*, 141–155. https://doi.org/10.1016/j.ocecoaman.2017.07.011

Masselink, G., Russell, P., Turner, I., & Blenkinsopp, C. (2009). Net sediment transport and morphological change in the swash zone of a high-energy sandy beach from swash event to tidal cycle time scales. *Marine Geology*, *267*(1–2), 18–35. https://doi.org/10.1016/j.margeo.2009.09.003

Meza-Valle, C. (2024). Wave-swash-interactions. (Release v1.0) [Dataset and software]. https://doi.org/10.5281/zenodo.12699739

Mordant, N., Crawford, A. M., & Bodenschatz, E. (2004). Experimental Lagrangian acceleration probability density function measurement. *Physica D*, *193*(1–4), 245–251. https://doi.org/10.1016/j.physd.2004.01.041

O'Donoghue, T., Kikkert, G. A., andN. Dodd, D. P., & Briganti, R. (2016). Intra-swash hydrodynamics and sediment flux for dambreak swash on coarse-grained beaches. *Coastal Engineering*, *112*, 113–130. https://doi.org/10.1016/j.coastaleng.2016.03.004

O'Donoghue, T., Pokrajac, D., & Hondebrink, L. J. (2010). Laboratory and numerical study of dambreak-generated swash on impermeable slopes. *Coastal Engineering*, *57*(5), 513–530. https://doi.org/10.1016/j.coastaleng.2009.12.007

Park, Y. (2009). *Seabed dynamics and breaking waves* (Doctoral Dissertation). Cornell University. Retrieved from https://hdl.handle.net/1813/14011

Pintado-Patiño, J. C., Puleo, J. A., Krafft, D., & Torres-Freyermuth, A. (2021). Hydrodynamics and sediment transport under a dam-break-driven swash: An experimental study. *Coastal Engineering*, *170*(103986), 1–18. https://doi.org/10.1016/j.coastaleng.2021.103986

Pujara, N., Clos, K. T. D., Ayres, S., Variano, E. A., & Karp-Boss, L. (2021). Measurements of trajectories and spatial distributions of diatoms (*Coscinodiscus* spp.) at dissipation scales of turbulence. *Experiments in Fluids*, *62*, 149. https://doi.org/10.1007/s00348-021-03240-5

Pujara, N., Liu, P. L.-F., & Yeh, H. (2015a). The swash of solitary waves on a plane beach: Flow evolution, bed shear stress and run-up. *Journal of Fluid Mechanics*, *779*, 556–597. https://doi.org/10.1017/jfm.2015.435

Pujara, N., Liu, P. L.-F., & Yeh, H. H. (2015b). An experimental study of the interaction of two successive solitary waves in the swash: A strongly interacting case and a weakly interacting case. *Coastal Engineering*, *105*, 66–74. https://doi.org/10.1016/j.coastaleng.2015.07.011

Puleo, J. A., Beach, R. A., Holman, R. A., & Allen, J. S. (2000). Swash zone sediment suspension and transport and the importance of bore-generated turbulence. *Journal of Geophysical Research*, *105*(C7), 17021–17044. https://doi.org/10.1029/2000JC900024

Puleo, J. A., & Butt, T. (2006). The first international workshop on swash-zone processes. *Continental Shelf Research*, *26*(5), 556–560. https://doi.org/10.1016/j.csr.2006.01.008

Puleo, J. A., & Torres-Freyermuth, A. (2016). The second international workshop on swash-zone processes. *Coastal Engineering*, *115*, 1–7. https://doi.org/10.1016/j.coastaleng.2015.09.007

21699291, 2024, 10, Downloaded from https://agupubs.onlinelibrary.wiley.com/doi/10.1029/2024JC021126 by Nimish Pujara - University Of Wisconsin , Wiley Online Library on [14/10/2024]. See the Terms and Conditions (https://onlinelibrary.wiley.com/terms-and-conditions) on Wiley Online Library for rules of use; OA articles are governed by the applicable Creative Commons License

Ruffini, G., Briganti, R., Alsina, J. M., Brocchini, M., Dodd, N., & McCall, R. (2020). Numerical modeling of flow and bed evolution of bichromatic wave groups on an intermediate beach using nonhydrostatic xbeach. *Journal of Waterway, Port, Coastal, and Ocean Engineering*, *146*(1), 04019034. https://doi.org/10.1061/(ASCE)WW.1943-5460.0000530

Smit, P., Stelling, G., Roelvink, D. J. A., van Thiel de Vries, J., McCall, R., van Dongeren, A., et al. (2010). *Xbeach: Non-hydrostatic model: Validation, verification and model description*. Deltares Technical Report.

Sou, I. M., & Yeh, H. (2011). Laboratory study of the cross-shore flow structure in the surf and swash zones. *Journal of Geophysical Research*, *116*(C03002), 1–15. https://doi.org/10.1029/2010JC006700

Stark, N., Mewis, P., Reeve, B., Florence, M., Piller, J., & Simon, J. (2022). Vertical pore pressure variations and geotechnical sediment properties at a sandy beach. *Coastal Engineering*, *172*(104058), 1–15. https://doi.org/10.1016/j.coastaleng.2021.104058

Sumer, B. M., Guner, H., Hansen, N. M., Fuhrman, D. R., & Fredsøe, J. (2013). Laboratory observations of flow and sediment transport induced by plunging regular waves. *Journal of Geophysical Research: Oceans*, *118*(11), 6161–6182. https://doi.org/10.1002/2013JC009324

Toimil, A., Camus, P., Losada, I. J., Cozannet, G. L., Nicholls, R. J., Idier, D., & Maspataud, A. (2020). Climate change-driven coastal erosion modelling in temperate sandy beaches: Methods and uncertainty treatment. *Earth-Science Reviews*, *202*, 103110. https://doi.org/10.1016/j.earscirev.2020.103110

Wu, Y.-T., Higuera, P., & Liu, P. L.-F. (2021). On the evolution and runup of a train of solitary waves on a uniform beach. *Coastal Engineering*, *170*, 104015. https://doi.org/10.1016/j.coastaleng.2021.104015

Yeh, H., & Ghazali, A. (1988). On bore collapse. *Journal of Geophysical Research*, *93*(C6), 6930–6936. https://doi.org/10.1029/JC093iC06p06930

21699291, 2024, 10, Downloaded from https://agupubs.onlinelibrary.wiley.com/doi/10.1029/2024JC021126 by Nimish Pujara - University Of Wisconsin , Wiley Online Library on [14/10/2024]. See the Terms and Conditions (https://onlinelibrary.wiley.com/terms-and-conditions) on Wiley Online Library for rules of use; OA articles are governed by the applicable Creative Commons License